Chapter 9

Complex Wavenumber Fourier Analysis of Hierarchic P-Version and Spectral Finite Elements

In recent years, there has been a resurgence of interest in the use of hierarchical p-version finite element and spectral elements to obtain high-resolution numerical solutions for wave propagation problems. In this chapter we show that high-order finite element discretizations of the wave equation display frequency bands where the solutions are harmonic decaying waves. In these so called 'stopping' bands, the solutions are not purely propagating (real wavenumbers) but are attenuated (complex wavenumbers). In this work, the standard dispersion analysis technique is extended to include complex wavenumbers. This new complex wavenumber Fourier analysis technique is then used to examine the dispersion and attenuation characteristics of high-order finite element discretizations. Three types of high-order elements are considered: hierarchic p-version elements with Legendre basis functions; new hierarchic Fourier elements with sinusoidal basis functions, and spectral elements with Lagrange interpolation in conjunction with Gauss-Lobatto quadrature. Practical guidelines are reported for phase and amplitude accuracy in terms of the spectral order and the number of elements per wavelength. Results from this analysis provide a guide for the design of p- and hp-version adaptive schemes, high-order preconditioners for iterative solution methods, and the selection of optimal Galerkin/Least-Squares (GLS) mesh parameters for elements using high-order basis functions.

9.1 Background

Computational methods for solving vibration and wave propagation problems introduce errors which distort the physical nature of the computed wave motion. Describing those errors by invoking concepts which originated in mathematical physics, such as dispersion and amplitude attenuation has provided a greater understanding of the numerical methods. In this respect, Fourier analysis has provided an indispensable tool for measuring the accuracy of wave propagation traveling through a finite element spatial discretization of a continuum. Previous researchers in this area have generally restricted themselves to studying the ability of the finite element spatial discretization to admit purely propagating wave solutions. This type of analysis amounts to a discrete Fourier synthesis of the finite element method with pure real wavenumbers. The information obtained from real wavenumber Fourier analysis has been used by by several researchers to study the accuracy of finite element discretizations. Some examples are the works of Belytschko and Mindle [1980a], Mindle and Belytschko [1983] and Jasti [1992] where the effect of various mass approximation techniques on the accuracy of Bernoulli-Euler and Timoshenko beam elements were considered. Underwood [1974] used real wavenumber analysis to study axisymmetric shells and rings, while Park and Flaggs [1984,1985] applied this technique to study shear locking and spurious modes found in Reissner/Mindlin plate elements. Real wavenumber Fourier analysis has also been used to study the convergence rates of equation solving algorithms, e.g Lotstedt and Gustafsson [1993].

While discretizations based on elements with linear basis functions represent popular element families due to their computational efficiency, higher-order elements such as quadratic interpolations offer special advantages when solving wave propagation problems. Higher-order elements better approximate the geometric curvature of a model description, and it is shown in this work that increased phase accuracy may be realized by employing higher-order interpolation fields.

To date, most of the effort in the study of the dispersive characteristics of finite element discretization has been limited to low-order elements. The most notable exception is the real wavenumber dispersion analysis of a quadratic bar element performed by Belytschko and Mullen [1978]. In this study, the dispersion analysis revealed the existence of a ‘stopping’ band in the frequency spectrum of quadratic elements, where solutions in this frequency range decay exponentially. The ramifications of these stopping bands in the context of finite element analysis were not fully understood, although there is some discussion in Belytschko and Mullen [1978] and Abboud and Pinsky [1992]. In order to obtain finite element dispersion relations for high-order finite element discretizations and interpret the solution within the 'stopping' bands, the traditional approach to finite element Fourier analysis must be extended. The standard approach seeks real frequencies as a function of real wavenumber.

In Thompson and Pinsky [1993a,1993b] the technique of complex wavenumber Fourier analysis is used to examine the accuracy of various high-order finite element discretizations. Complex wavenumber Fourier analysis is discussed in the context of periodic structures in Brillouin [1953]. In this approach the standard Fourier analysis technique is extended to include all wavenumbers satisfying the finite element dispersion relation, either real, imaginary or complex. The complex wavenumber may correspond to either a propagating wave (real wavenumber), evanescent wave (imaginary wavenumber), or a harmonic decaying wave (complex wavenumber). This extension of the usual procedure involves only a slight modification to the standard Fourier analysis yet allows for a complete characterization of the 'stopping' band phenomena found in higher order finite element discretizations – a characterization that has previously escaped other analysts.

Other applications of complex wavenumber Fourier analysis include the works of Harari and Hughes [1991a,b] where amplitude errors caused by purely imaginary wavenumbers found in the dispersion relation for linear finite element discretizations are examined. This type of analysis can also be used to investigate other systems where complex wavenumbers are present, such as periodic composite structures Silva [1991] and the study of the subsonic, leaky and evanescent waves present in the finite element dispersion relations for fluid-loaded plates Jasti [1992],Grosh and Pinsky [1993a].

In recent years, there has been a resurgence of interest in elements of high degree, see for example Babuska and Suri [1990] and Maday and Patera [1989]. In p–refinement the effects of numerical dispersion can be minimized by increasing the spectral order p of the finite element interpolation functions, while holding the number of elements constant. In contrast, standard h-refinement is achieved by holding the spectral order fixed while increasing the number of elements. The h- and p-versions are just special applications of the finite element method, which allows changing the mesh concurrently with increasing the spectral order p; this general approach is called the hp-version. The complex Fourier analysis performed in this thesis will characterize the accuracy in terms of both h and p refinements over the entire range of complex wavenumbers. Three different p–extensions are considered: (a) Hierarchic Legendre basis functions, (b) Hierarchic Fourier basis functions, and (c) Lagrange interpolations together with Lobatto quadrature.

Results from this analysis provides a guide for adaptive solution schemes in the form of an *a priori* error estimate. For example, the dispersion error determined from the analysis of high-order methods could be used as a measure for selecting the required spectral order and mesh size at a given frequency in an adaptive solution. Results from the analysis can also be used to design efficient high order preconditioners for iterative solution techniques such as those used in Babuska, et al. [1991], Barragy and Carey [1991], and Deville and Mund [1992].

9.2 Overview

In Section 9.3 the analytic Fourier analysis of the continuous problem in one-dimension is reviewed. The resulting analytic dispersion curves will serve as a basis for comparison to the discrete dispersion curves obtained from a complex wavenumber Fourier synthesis of high-order finite element discretizations. Finite element matrix equations arising from the use of high-order basis functions are given in Section 9.4. In Section 9.5 we extend the standard finite element dispersion analysis to include complex wavenumbers in order to obtain the complex valued roots of the finite element dispersion relation for the three alternative basis functions considered. Results of the dispersion and attenuation analysis are reported in Section 9.6. Of particular interest is the presence of complex wavenumber bands (stopping bands) that occur in these high-order elements and the determination of their practical significance. In Section 9.7 a direct connection is established between the results from the Fourier analysis and the results obtained from the solution of a simple canonical boundary-value problem. We also indicate how information obtained from the Fourier analysis can be used as a tool to help improve the eigenmodes from a vibration problem through a simple post-processing exercise.

9.3 Fourier analysis of the Continuous Problem

Consider the steady-state response, ϕ for the one-dimensional reduced wave (Helmholtz) equation,

$$\frac{d^2\phi(x)}{dx^2} + \frac{\omega^2}{c^2}\phi(x) = f \tag{9.1}$$

where c is the wave speed, and f is the forcing function. with assumed time dependence $e^{-i\omega t}$; and ω is the circular frequency. The Fourier analysis of the reduced wave equation is accomplished by transforming the problem from the spatial (x) domain to the wavenumber domain (k) by seeking complex exponential solutions for ϕ of the form,

$$\phi(x) = A\mathrm{e}^{ikx} \tag{9.2}$$

with constant amplitude $|\phi| = A$. We interpret the spatial contribution to the wave solution as the integrand of the Fourier transformation in which the wavenumber k represents the continuous spatial frequency with wavelength $2\pi/k$. The complex Fourier transform is defined as,

$$\tilde{F}(k) := \frac{1}{\sqrt{2\pi}}\int_{-\infty}^{\infty} F(x)\mathrm{e}^{-ikx}\, dx \tag{9.3}$$

Substituting the complex exponential solution (9.2) into the homogeneous form of (9.1), or equivalently applying the complex Fourier transform (9.3), we obtain its characteristic equation in the nondimensional form,

$$\boxed{(kh)^2 = (\omega h/c)^2} \tag{9.4}$$

where h is a problem dependent characteristic length. The properties of the solutions to (9.4) are: (a) The nondimensional wavenumber (kh) is linearly proportional to the nondimensional frequency ($\omega h/c$) over all frequencies, and (b) The wavenumbers occur in pairs $\pm kh$ of purely real numbers corresponding to propagating free waves in both $\pm x$ directions. With c constant, the phase velocity is independent of frequency and the medium is nondispersive.

In contrast to the continuum problem, we will find that finite element solutions have a dispersive character. Many naturally occurring discrete systems exhibit similar dispersive properties. Examples include periodic lattices of polyatomic molecules studied by Brillouin [1953], and periodic composite structures studied by Silva [1991] and others.

9.4 High-order Finite Element Discretizations

In this section we describe a discrete Fourier transform counterpart to the analytical Fourier transform (9.3). It will be applied to the finite element discretization of the continuous problem in one-dimension, in order to obtain a characteristic equation relating frequency and wavenumber. Since the wavenumbers obtained through the discrete Fourier transform are in general complex, we are able to obtain real, imaginary or complex wavenumber solutions. The analysis is demonstrated for the one-dimensional Helmholtz equation, however results obtained from studying this equation are useful for multi-dimensional discretizations where spatial variations and wave propagation are restricted to one dimension. For Fourier analysis, we are interested in the infinite domain $\Omega = (-\infty, \infty)$, so that no end-point boundary conditions are considered.

Consider the higher-order finite element approximation of the solution,

$$\boxed{\phi^h(\xi) = \sum_{a=1}^{p+1} N_a(\xi)\phi_a \qquad \xi \in [-1, 1]} \tag{9.5}$$

where $N_a(\xi)$ are shape functions with compact support defined in the local element coordinate ξ, and p is the spectral order. Three different finite element approximations are considered : (1) Hierarchic Legendre shape functions, (2) New Hierarchic Fourier shape functions, and (3) Lagrange shape functions in conjunction with Lobatto quadrature.

Upon introducing the higher-order interpolations defined in (9.5) into the Galerkin/least-squares variational equation for this one-dimensional problem we obtain the following symmetric element impedance matrix,

$$\boldsymbol{s}^e = [s^e_{ab}] \in \mathbb{R}^{(p+1)\times(p+1)} \qquad a, b = 1 : p+1 \tag{9.6}$$

$$\boxed{\boldsymbol{s}^e = \boldsymbol{k}^e - (1 - \tau k^2)k^2 \boldsymbol{m}^e + \tau \hat{\boldsymbol{k}}^e + \tau k^2 \bar{\boldsymbol{k}}^e} \tag{9.7}$$

where $k = \omega/c$ and

$$\begin{aligned} k^e_{ab} &= (N_{a,x}\,,\, N_{b,x})_{\Omega_e} \\ m^e_{ab} &= (N_a\,,\, N_b)_{\Omega_e} \\ \hat{k}^e_{ab} &= (N_{a,xx}\,,\, N_{b,xx})_{\Omega_e} \\ \bar{k}^e_{ab} &= (N_{a,xx}\,,\, N_b)_{\Omega_e} + (N_a, N_{b,xx})_{\Omega_e} \end{aligned}$$

and the L_2 inner product is defined as,

$$(N_a\,,\, N_b)_{\Omega_e} = \frac{h}{2}\int_{-1}^{1} N_a N_b d\xi \tag{9.8}$$

where h is the element length. In the above expressions, $\boldsymbol{k}^e$ and $\boldsymbol{m}^e$ are the local stiffness and mass matrices emanating from the Galerkin formulation, while the matrices $\hat{\boldsymbol{k}}^e$ and $\bar{\boldsymbol{k}}^e$ are additional contributions obtained from the Least-Squares terms.

9.4.1 P-Version Hierarchic Legendre Elements

Let $\mathcal{S}^p \subset H^1$ be the finite element subspace of continuous piecewise polynomials of degree p denoted by $\mathcal{P}^p$.

$$\mathcal{S}^p = \{\phi | \phi \in C^o(\Omega), \phi \in \mathcal{P}^p(\Omega_e)\}$$

The basis functions used in the p-version finite element method are obtained by starting with the standard linear nodal shape functions,

$$N_a(\xi) = \frac{1}{2}(1 + \xi_a \xi) \qquad a = 1, 2 \tag{9.9}$$

and then adding in a hierarchical fashion internal shape functions defined in terms of integrals of Legendre polynomials.

$$\boxed{N_a(\xi) := \frac{1}{||P_{a-2}||} \int_{-1}^{\xi} P_{a-2}(\xi')d\xi', \qquad a = 3, 4, \cdots, p+1} \tag{9.10}$$

with the norm of the Legendre polynomial,

$$||P_{a-2}||^2 = \frac{2}{2a-3} \tag{9.11}$$

These functions are constructed such that $N_a(\pm 1) = 0$. As a result of this property the variables $\phi_1 = \phi^h(-1)$ and $\phi_2 = \phi^h(1)$ define discrete nodal variables, while the values $\phi_a, a \geq 3$ compose a set of internal variables. The derivatives of these hierarchical functions form an orthonormal basis with the property,

$$\int_{-1}^{1} \frac{dN_a}{d\xi}\frac{dN_b}{d\xi} d\xi = \delta_{ab} \qquad a, b = 3 : p+1 \tag{9.12}$$

As a result of this orthogonality property, the local element stiffness matrix is diagonal beyond $a > 2$. For example, for $p = 6$, the symmetric hierarchical element stiffness matrix is,

$$\boldsymbol{k} = \boldsymbol{k}^T = \frac{1}{h} \begin{bmatrix} 1 & -1 & 0 & 0 & 0 & 0 & 0 \\ & 1 & 0 & 0 & 0 & 0 & 0 \\ & & 2 & 0 & 0 & 0 & 0 \\ & & & 2 & 0 & 0 & 0 \\ & & & & 2 & 0 & 0 \\ & & & & & 2 & 0 \\ & & & & & & 2 \end{bmatrix} \tag{9.13}$$

The hierarchical mass matrix in this case is,

$$\boldsymbol{m} = \boldsymbol{m}^T = \frac{h}{6}\begin{bmatrix} 2 & 1 & -\frac{3}{\sqrt{6}} & \frac{1}{\sqrt{10}} & 0 & 0 & 0 \\ & 2 & -\frac{3}{\sqrt{6}} & -\frac{1}{\sqrt{10}} & 0 & 0 & 0 \\ & & \frac{6}{5} & 0 & -\frac{3}{5\sqrt{21}} & 0 & 0 \\ & & & \frac{2}{7} & 0 & -\frac{3}{7\sqrt{45}} & 0 \\ & & & & \frac{2}{15} & 0 & -\frac{1}{3\sqrt{77}} \\ & & & & & \frac{6}{77} & 0 \\ & & & & & & \frac{2}{39} \end{bmatrix} \tag{9.14}$$

For $p \geq 2$ the diagonal mass coefficients are,

$$m^e_{aa} = \frac{h}{(2a-1)(2a-5)}, \qquad a \geq 3 \tag{9.15}$$

The off-diagonal terms are zero for $p \geq 2$, except:

$$m^e_{a,a+2} = m^e_{a+2,a} = \frac{-h}{2(2a-1)\sqrt{(2a-3)(2a+1)}} \qquad a \geq 3 \tag{9.16}$$

Note that the upper left (2×2) partition is the standard linear ($p = 1$) element matrix. The element matrices are hierarchic in the sense that the matrix corresponding to $\mathcal{S}^p$ is embedded in the matrix corresponding to $\mathcal{S}^{p+1}$.

9.4.2 New Hierarchic Fourier Elements

Examining the propagating solution to the Helmholtz problem, I have hypothesized that the introduction of trigonometric basis functions should be a better approximation to the complex exponential solution, compared to the polynomial interpolation used in the Legendre based elements. In this case consider hierarchic elements that start with the standard linear nodal shape functions defined in (9.9) and then add to these in a hierarchical manner internal shape functions defined in terms of the Fourier modes,

$$\boxed{N_a(\xi) = \frac{2}{(a-2)\pi}\sin((a-2)(1+\xi)\pi/2) \qquad a = 3, 4, \cdots, p+1} \tag{9.17}$$

These functions satisfy $N_a(\pm 1) = 0$ and the orthogonality properties,

$$\int_{-1}^{1} N_a N_b d\xi = \frac{2}{(a-2)\pi}\delta_{ab}; \qquad \int_{-1}^{1} \frac{dN_a}{d\xi}\frac{dN_b}{d\xi} d\xi = \delta_{ab} \tag{9.18}$$

As a result of this normalization, the local element stiffness matrix is identical to the stiffness matrix obtained with the Legendre polynomial based elements. However, the use of Fourier modes changes the mass matrix. For $p \geq 2$ the diagonal mass coefficients in this case are,

$$m^e_{aa} = \frac{2h}{(a-2)^2\pi^2}, \qquad a \geq 3 \tag{9.19}$$

The off-diagonal terms are zero except for the first two rows (columns),

$$m^e_{1a} = m^e_{a1} = m^e_{aa}, \qquad a \geq 3 \tag{9.20}$$

$$m^e_{2a} = m^e_{a2} = (-1)^{a+1} m^e_{aa}, \qquad a \geq 3 \tag{9.21}$$

For example, the hierarchical element mass matrix for $p = 6$ is,

$$\boldsymbol{m} = \boldsymbol{m}^T = \frac{h}{6\pi^2}\begin{bmatrix} 2\pi^2 & \pi^2 & 12 & 3 & \frac{4}{3} & \frac{3}{4} & \frac{12}{25} \\ & 2\pi^2 & 12 & -3 & \frac{4}{3} & -\frac{3}{4} & \frac{12}{25} \\ & & 12 & 0 & 0 & 0 & 0 \\ & & & 3 & 0 & 0 & 0 \\ & & & & \frac{4}{3} & 0 & 0 \\ & & & & & \frac{3}{4} & 0 \\ & & & & & & \frac{12}{25} \end{bmatrix} \tag{9.22}$$

Comparing this mass matrix to the mass matrix using Legendre polynomials; the effect of using Fourier modes is to change the hierarchical terms in the mass matrix from a tri-diagonal matrix, to a diagonal matrix with a full block of coupling terms in the first two rows (columns).

9.4.3 Spectral elements

Higher-order elements based on Lagrange interpolation polynomials in conjunction with Gauss-Lobotto quadrature lead to the so-called 'spectral elements' when used with a high spectral order p, see e.g. Patera [1984], Maday and Patera [1989], and Fischer and Patera [1991]. These spectral elements are designed to combine the geometric flexibility of the standard finite element techniques with the rapid convergence rate of global spectral schemes. For a general overview of spectral methods see Voight et al. [1984] and Canuto et al. [1988].

In the spectral element method, the solution variable ϕ^h is expanded within each element in terms of high-order Lagrangian interpolants, $N_a(\xi) \in \mathcal{P}^p$:

$$\{N_a(\xi) \in \mathcal{P}^p,\, N_a(\xi_b) = \delta_{ab}\; \forall a, b \in \{1, \cdots, p+1\}\} \tag{9.23}$$

evaluated at $p+1$ Gauss-Lobatto points such that $\xi_1 = -1$ and $\xi_{p+1} = 1$, with the other points being obtained as the roots of the derivative of the Legendre polynomials. Gauss-Lobatto points ξ_a, and their corresponding weight factors W_a can be found in tables Szabo and Babuska [1991], or computed directly from subroutine libraries see Canuto et al. [1988]. In this case, the solution variables are all nodal values, $\phi_a = \phi^h(\xi_a)$, and the basis is not hierarchical. The local matrices for these elements are,

$$k^e_{ab} = \frac{2}{h}\sum_{q=1}^{p+1} N'_a(\xi_q)N'_b(\xi_q)W_q \tag{9.24}$$

$$m^e_{ab} = \frac{h}{2}\sum_{q=1}^{p+1} N_a(\xi_q)N_b(\xi_q)W_q = \frac{h}{2}\,\delta_{ab}\,W_a \tag{9.25}$$

$$\hat{k}^e_{ab} = \frac{8}{h^3}\sum_{q=1}^{p+1} N''_a(\xi_q)N''_b(\xi_q)W_q \tag{9.26}$$

$$\bar{k}^e_{ab} = \frac{2}{h}\sum_{q=1}^{p+1} N''_a(\xi_q)N_b(\xi_q)W_q + \frac{2}{h}\sum_{q=1}^{p+1} N_a(\xi_q)N''_b(\xi_q)W_q \tag{9.27}$$

By choice of Gauss-Lobatto quadrature, the elemental mass matrix is underintegrated and diagonal.

$$\boldsymbol{m} = \boldsymbol{m}^T = \frac{h}{2}\mathrm{diag}(W_a), \qquad a = 1, 2, \cdots, p+1 \tag{9.28}$$

9.5 Complex Wavenumber Fourier Analysis

In this section a complex wavenumber Fourier analysis technique is developed to investigate the dispersive and attenuation properties of higher-order finite elements. The method employs only a minor modification to the technique of real wavenumber analysis but is completely general, and can accommodate any finite element discretization and spectral order. In the present analysis, attention is restricted to Galerkin discretizations with $\tau = 0$.

9.5.1 The Schur Complement

Before the assembly of the finite element equations, for hierarchical elements, it is necessary to decouple the degrees of freedom associated with the interior of the element domain from the element dynamic stiffness (impedance) matrix. This process of condensation reduces the system of dynamic equations to nodal (physical) variables only. This is a necessary prelude to the discrete Fourier transform, where complex exponential solutions are assumed at discrete nodes (sampling points).

The frequency dependent dynamic stiffness matrix $\boldsymbol{s}^e$ is partitioned into the following matrix block form,

$$\boldsymbol{s}^e = \begin{bmatrix} \boldsymbol{s}_{11} & \boldsymbol{s}_{12} \\ \boldsymbol{s}_{12}^T & \boldsymbol{s}_{22} \end{bmatrix} \in \mathbb{R}^{(p+1)\times(p+1)} \tag{9.29}$$

The matrix partition $\boldsymbol{s}_{22} \in \mathbb{R}^{(p-1)\times(p-1)}$ corresponds to interactions among internal shape functions, $\boldsymbol{s}_{12} \in \mathbb{R}^{2\times(p-1)}$ is the coupling matrix partition due to interactions between internal shape functions and nodal shape functions, and finally, $\boldsymbol{s}_{11} \in \mathbb{R}^{2\times 2}$ corresponds to interactions among the nodal shape functions N_1 and N_2. Using the Schur complement,

$$\boldsymbol{g}^e = \boldsymbol{s}_{11} - \boldsymbol{s}_{12}\boldsymbol{s}_{22}^{-1}\boldsymbol{s}_{12}^T, \qquad \boldsymbol{g}^e \in \mathbb{R}^{2\times 2} \tag{9.30}$$

We obtain the condensed element dynamic stiffness $\boldsymbol{g}^e$ that couples only the two element nodal (i.e. physical) degrees of freedom. For $p \geq 2$ we obtain $\boldsymbol{g}^e$ symbolically using Mathematica, (WOLFRAM [1991]). Consider an infinite uniform mesh with equal element lengths h. Assembly of the condensed element dynamic stiffness matrices results in a tridiagonal system of linear equations of the form:

$$\boldsymbol{G}\boldsymbol{\phi} = 0, \qquad \boldsymbol{G} = \mathop{\mathbf{A}}_{e=1}^{n_{el}} \boldsymbol{g}^e \tag{9.31}$$

where $\boldsymbol{\phi}$ is the displacement solution vector, and $\mathop{\mathbf{A}}_{e=1}^{n_{el}}$ is the assembly operator. For present purposes, no source terms are included. The nth equation of this tridiagonal system is a stencil of the form:

$$\boxed{G_1(\alpha)\phi_{n-1} - 2G_2(\alpha)\phi_n + G_1(\alpha)\phi_{n+1} = 0} \tag{9.32}$$

All other equations are a repetition of this stencil. In this difference stencil, the coefficients $G_1(\alpha)$ and $G_2(\alpha)$ are polynomials of degree $2p$ in the nondimensional frequency:

$$\boxed{\alpha = \omega h/c} \tag{9.33}$$

For linear elements ($p = 1$), we recover the difference coefficients of standard consistent and diagonal mass finite element approximations,

$$G_1(\alpha) = 1 + \epsilon\alpha^2/6, \qquad G_2(\alpha) = 1 - (3 - \epsilon)\alpha^2/6 \tag{9.34}$$

The constant ϵ is a mass approximation parameter equal to 1 for exactly integrated (consistent) mass, and 0 for Lobatto integrated (diagonal) mass.

The structure of the stencil is seen by writing (9.32) in the difference operator form,

$$\boxed{F(\alpha)\phi_n = 0} \tag{9.35}$$

where,

$$F(\alpha) = \sum_{j=-1}^{1} F_j(\alpha)E_j \tag{9.36}$$

is a second order linear difference operator and E_j is a shift operator with the property

$E_j\phi_n = \phi_{n+j}$. The symmetric frequency dependent coefficients are,

$$\begin{aligned} F_1(\alpha) &= G_1(\alpha) = F_{-1}(\alpha) \\ F_0(\alpha) &= -2G_2(\alpha) \end{aligned}$$

9.5.2 Characteristic equation for high-order elements

In analogy with (9.2), an exponential solution to (9.35) is assumed having the form:

$$\phi_n = A\mathrm{e}^{ik^h x_n}, \quad x_n = nh \tag{9.37}$$

where $k^h \in \mathbb{C}$ is the complex valued numerical wavenumber and $i = \sqrt{-1}$. Substitution of (9.37) into (9.35) results in the characteristic function,

$$\tilde{F}(\alpha,\beta) = \sum_{j=-1}^{1} F_j(\alpha)\mathrm{e}^{ij\beta} = 0 \tag{9.38}$$

where $\tilde{F}(\alpha,\beta)$ may be identified as the discrete Fourier transform of the linear difference operator F, α is the normalized frequency, and β is the normalized discrete wavenumber:

$$\boxed{\beta = k^h h} \tag{9.39}$$

Due to the symmetric form of ($F_1 = F_{-1}$), we find that $\tilde{F}$ is an even function resulting in the wavenumber-frequency relation,

$$\boxed{\cos(\beta) = \lambda(\alpha)} \tag{9.40}$$

where

$$\lambda(\alpha) := \frac{G_2(\alpha)}{G_1(\alpha)} \tag{9.41}$$

and the real spectrum of β is periodic in 2π with aliasing, $\beta = \beta + 2\pi m$; $m \in \mathbb{Z}$.

At this point, we depart from the standard finite element dispersion technique in which real frequency roots of (9.40) are sought for a given real wavenumber. Instead, we seek all the wavenumber roots of (9.40) for a given real frequency. The complex roots $\beta \in \mathbb{C}$, of (9.40) are found using the complex arc cosine (Churchill et al.

[1976]),

$$\boxed{Re(\beta) + iIm(\beta) = -i\ln(\lambda(\alpha) + i\sqrt{1 - (\lambda(\alpha))^2})} \tag{9.42}$$

It is noted that the amplitude of the discrete nodal solution is,

$$|\phi_n| = |A|\mathrm{e}^{-Im(\beta)n} \tag{9.43}$$

where the imaginary part $Im(\beta)$ is seen to be an attenuation parameter.

9.6 Dispersion and Attenuation Results

In this section we discuss the complex wavenumbers that arise from the Fourier analysis of high-order finite elements up to spectral order $p = 5$. It will be shown that the finite element characteristic equation (9.40) admits pure real wavenumbers, (propagating solutions) only when the frequency falls within a finite number of bands called passing bands. The number of passing bands is equal to the spectral order p of the elements in the mesh. In addition it will be shown that there are p stopping bands where the wavenumbers are complex. The results in this section apply to Galerkin finite element discretizations with $\tau = 0$.

9.6.1 Low-order elements

For $p = 1$ there is only one passing band where the wavenumber is purely real. For frequencies lower than a limiting frequency called the cut-off frequency we obtain real solutions for β. The cut-off frequency for consistent mass is $\alpha_{max} = \sqrt{12}$ and for diagonal mass $\alpha_{max} = 2$. In the complex wavenumber plane, for frequencies below the cut-off, then $|\lambda| < 1$, and the characteristic equation is satisfied by,

$$Re(\beta) = \cos^{-1}(\lambda), \quad \text{and} \qquad Im(\beta) = 0 \tag{9.44}$$

For higher frequencies β is complex, since above the cut-off frequency, $|\lambda| > 1$, and the characteristic equation is satisfied by,

$$Re(\beta) = \pi, \quad \text{and} \qquad Im(\beta) = \cosh^{-1}(\lambda) \tag{9.45}$$

Figure 9.1 plots the frequency dependence of the real (propagating) and imaginary (decaying) components of the complex numerical wavenumber $k^h \in \mathbb{C}$. The real wavenumber corresponding to the cut-off frequency is called the spatial resolution limit. For $p = 1$, the limit of spatial resolution is two elements per wavelength or $Re(\beta) = \pi$. For frequencies between 0 and α_{max}, β is real, and for frequencies above the cut-off, the real part of the discrete wavenumber stays constant at $Re(\beta) = \pi$, while the imaginary part of the discrete wavenumber increases rapidly.

As a result, the amplitude from node to node along the mesh stays constant until the frequency reaches the cut-off. Above the cut-off the amplitude decays exponentially along the mesh,

$$\left|\frac{\phi_{n+1}}{\phi_n}\right| = \begin{cases} 1 & \alpha < \alpha_{max} \\ e^{-Im(\beta)} & \alpha > \alpha_{max} \end{cases}$$

This illustrates how the finite element mesh acts as a low-pass filter analogous to discrete signal processing of data; allowing propagation of all frequencies up to the cut-off frequency, while strongly attenuating frequencies above the cut-off frequency; see Thompson and Pinsky [1993a,b] for a plot of this amplitude spectrum.

9.6.2 Higher-order elements

For a uniform mesh of p–version finite elements with spectral order ($p = 2$), the frequency dependence of the real and imaginary parts of $k^h \in \mathbb{C}$ are plotted in Figure 9.2. In this case, there are two passing bands: one for frequencies between $0 < \alpha < \alpha_1$ and one for frequencies between $\alpha_2 < \alpha < \alpha_{max}$. Within these bands, there is a purely propagating solution with $|\lambda| < 1$ and the characteristic equation is satisfied by,

$$Re(\beta) = \cos^{-1}(\lambda), \quad \text{and} \qquad Im(\beta) = 0 \tag{9.46}$$

The dispersion curve in the lower passing band is called the acoustical branch and the upper passing band is referred to as the optical branch. These designations arise from the analogous branches found in a diatomic crystal lattice where the frequencies in the lower branch are of the same order of magnitude as acoustical or subsonic vibrations, and frequencies in the upper branch are of the order of magnitude of infrared frequencies, see Brillouin [1953]. For our discussions, we use these designations for the different branches, but attach no physical significance to their names.

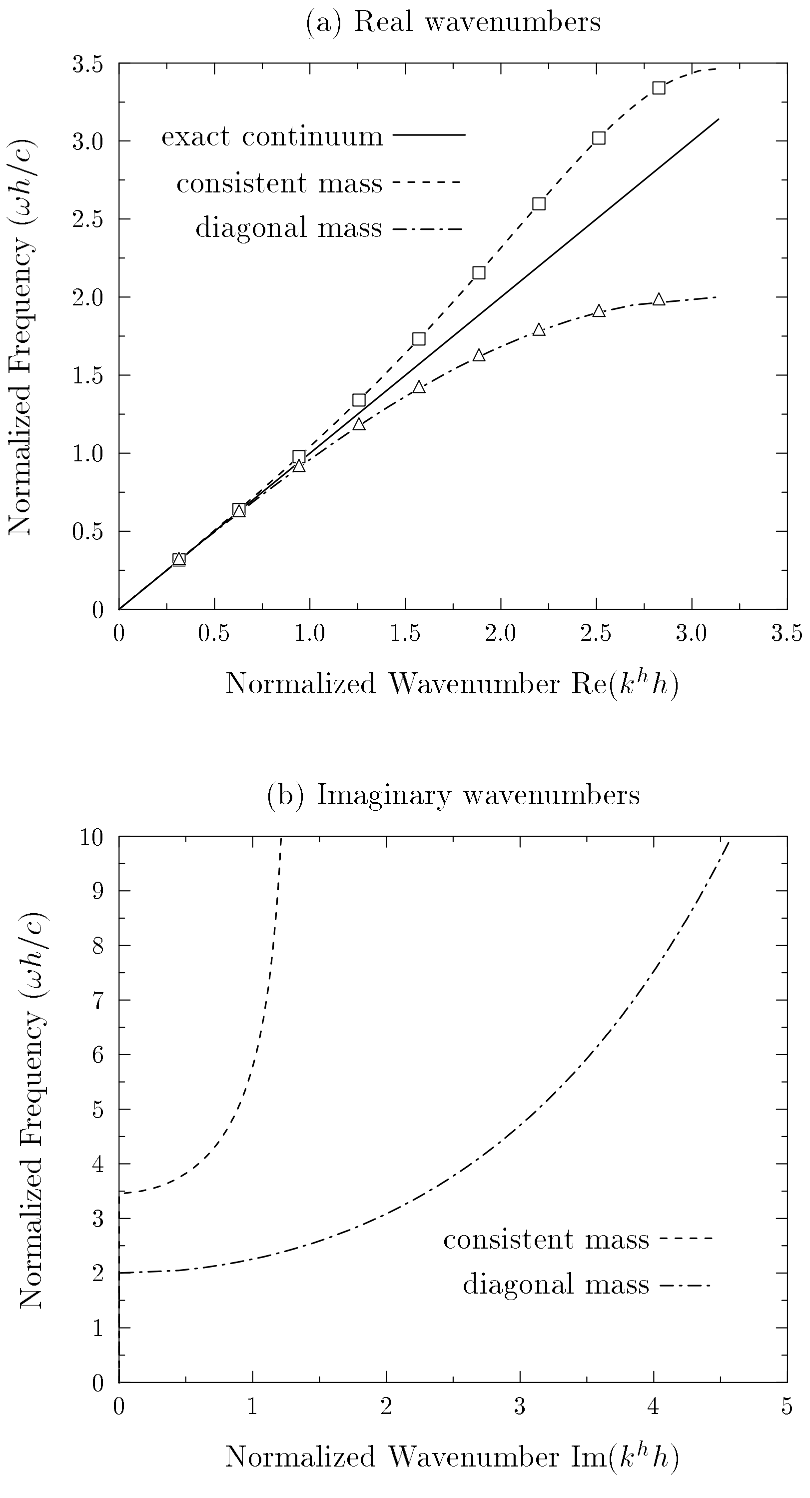

Figure 9.1: Frequency spectrum comparing linear finite element approximations obtained from Galerkin method: (a) Real wavenumbers, (b) Imaginary wavenumbers

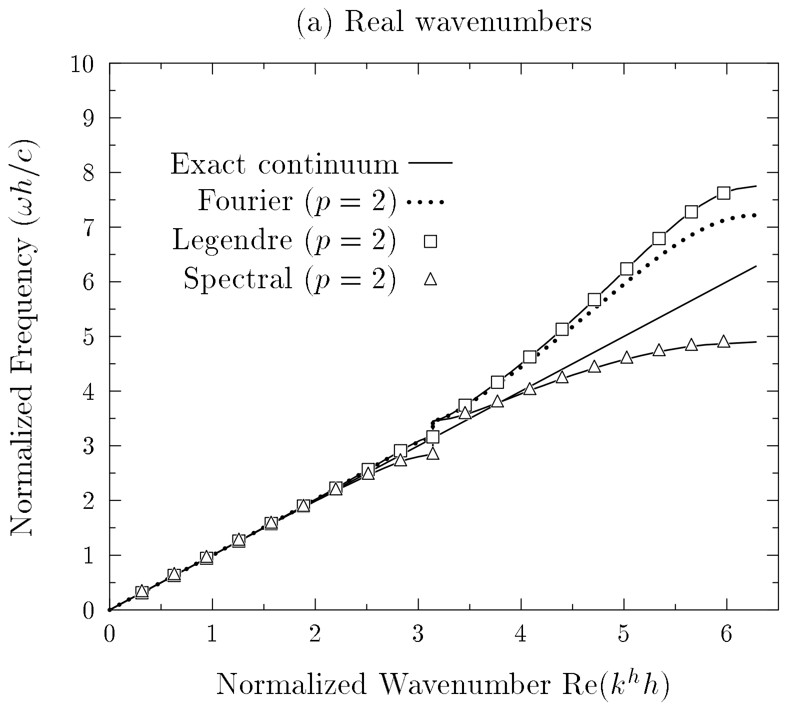

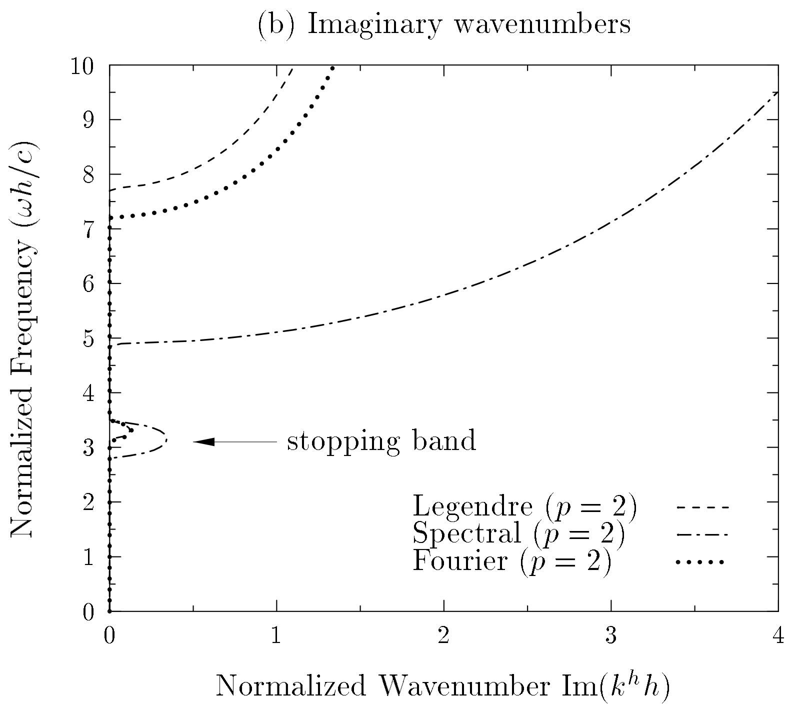

Figure 9.2: Frequency spectrum comparing quadratic finite element approximations obtained from Galerkin method: (a) Real wavenumbers, (b) Imaginary wavenumbers

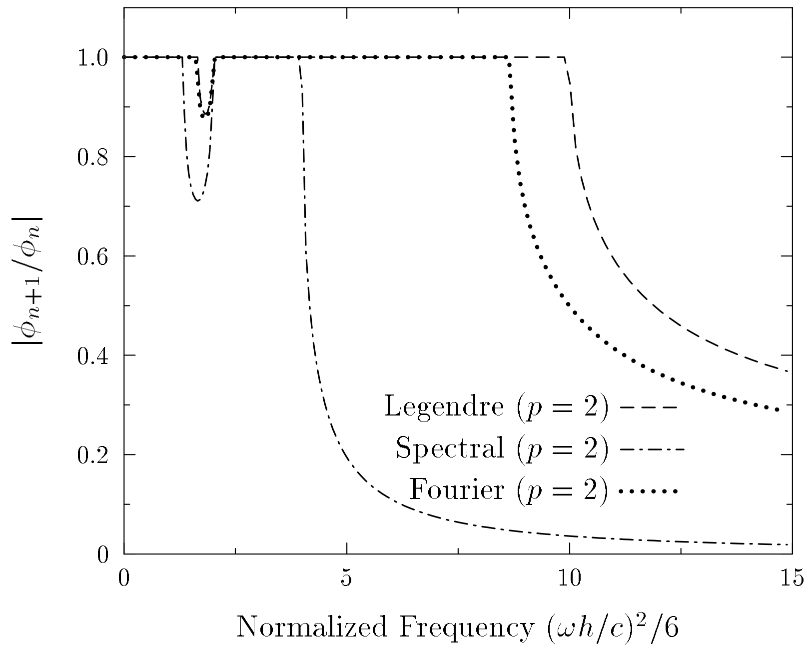

Figure 9.3: Amplitude spectrum for quadratic elements

In the frequency range between these two passing passing bands, $\alpha_1 \leq \alpha \leq \alpha_2$, there is one frequency band where the numerical wavenumbers are complex. In this band, $|\lambda| > 1$ and the characteristic equation is satisfied by,

$$Re(\beta) = \pi, \quad \text{and} \qquad Im(\beta) = \cosh^{-1}(-\lambda) \tag{9.47}$$

This complex wavenumber band is called a stopping band because in this frequency range, the real part of the wavenumber is constant and the imaginary component results in an attenuated wave solution with an amplitude decay proportional to the exponential of the imaginary wavenumber.

Above the cut-off frequency, $\alpha > \alpha_{max}$, $\lambda > 1$ and the characteristic equation is satisfied by,

$$Re(\beta) = 2\pi, \quad \text{and} \qquad Im(\beta) = \cosh^{-1}(\lambda) \tag{9.48}$$

In this case, the solution propagates with a fixed wavelength equal to the limit of resolution – one quadratic element per wavelength or $Re(\beta) = 2\pi$ with strong exponential amplitude decay from node to node along the mesh.

The amplitude spectrum for $p = 2$ is plotted in Figure 9.3. The amplitude ratio is constant in the first passing band (acoustical branch) up to the complex wavenumber band where the imaginary wavenumber components produce an amplitude decay. In the stopping band, the amplitude is attenuated until a minimum is reached and then increases back up to the exact ratio of one. The amplitude ratio continues to be exact throughout the second passing band (optical branch) until it reaches the cut-off where it is strongly attenuated. The cutoff frequency for the Spectral element falls well below that of the Legendre and Fourier elements.

Again invoking the signal processing analogy, the character of this amplitude spectrum illustrates how the p–version finite element mesh acts as a band-pass filter – allowing propagation of all frequencies in the passing bands, while weakly attenuating frequencies in the complex wavenumber band, and strongly attenuating frequencies above the cut-off frequency.

As the spectral order is increased to $p = 3$, the spatial resolution limit extends to $Re(\beta) = 3\pi$. Figure 9.4 shows that there are 3 passing and 3 stopping bands present in the frequency spectrum. The first complex wavenumber band occurs when $Re(\beta) = \pi$. The frequency range for the first stopping band is very small and appears as a small perturbation in the frequency curve for the imaginary wavenumber component at approximately $\alpha = \pi$, see Figure 9.4. The second stopping band occurs when the real wavenumber component reaches 2π and is much larger, with large imaginary wavenumber components present.

As a result of these complex wavenumber bands, we observe the amplitude attenuation characteristics shown in Figure 9.5(top). The amplitude ratio is again constant in the passing bands up to the first complex wavenumber band, where there is a very small attenuation loss. Isolating this frequency region in Figure 9.5(bottom), we observe that the maximum amplitude error is only 2.5 percent for the Spectral elements and only 1 percent for Legendre and Fourier elements. Thus in this first complex wavenumber region waves propagate with constant wavenumber $Re(\beta)$ and only a very small amplitude decay. The amplitude attenuation in the second complex frequency band is very large and in practice the element size h should be chosen to avoid this nondimensional frequency range.

These observations are extended to higher spectral orders as well. Results for spectral orders $p = 4$ and $p = 5$ are shown in Figure 9.6. For nondimensional frequencies up to $\alpha = (p-2)\pi$, the dispersion curves approximate the exact line with slope one. As the nondimensional frequency increases, the Legendre and Spectral

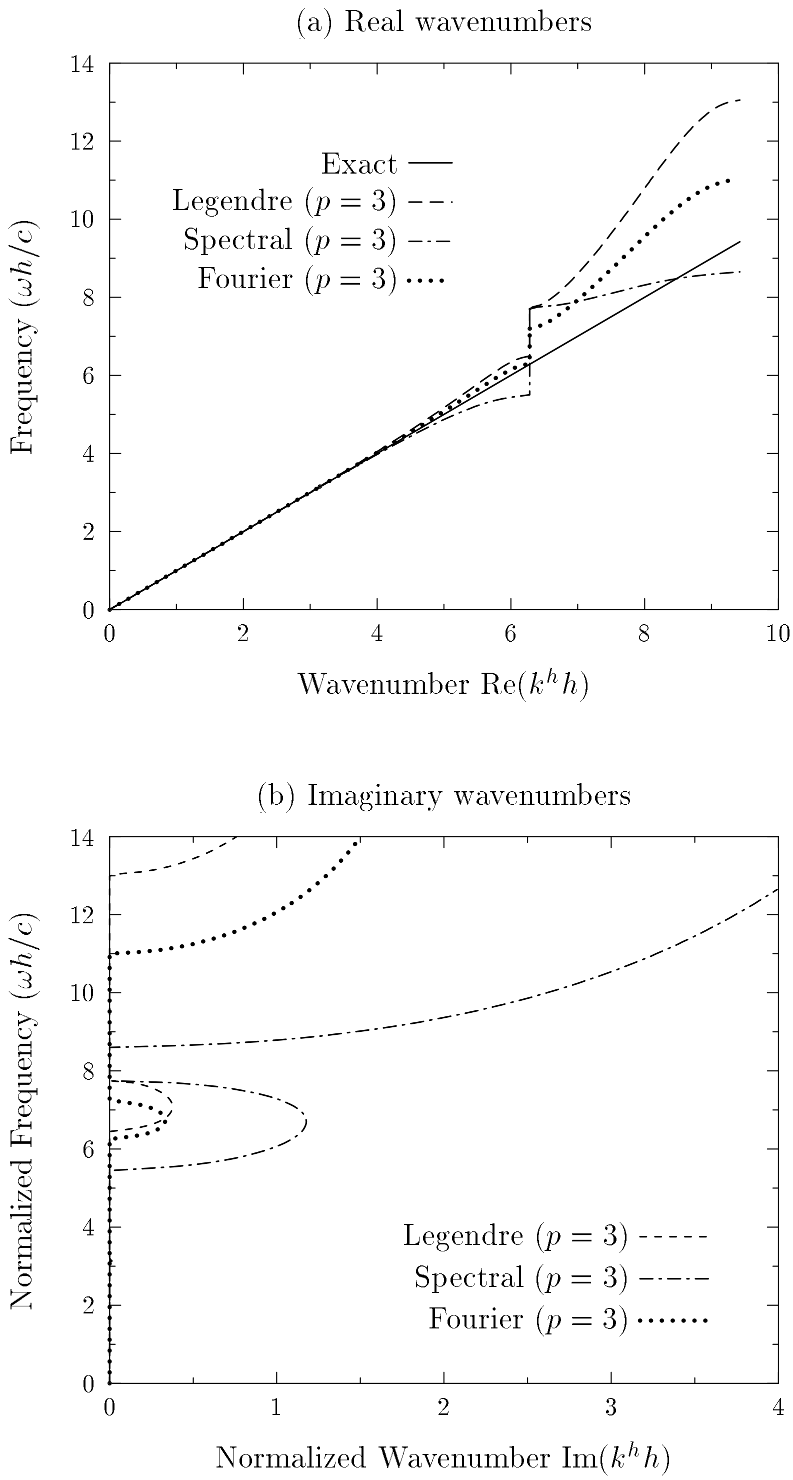

Figure 9.4: Frequency spectrum comparing cubic finite element approximations obtained from the Galerkin method: (a) Real wavenumbers, (b) Imaginary wavenumbers

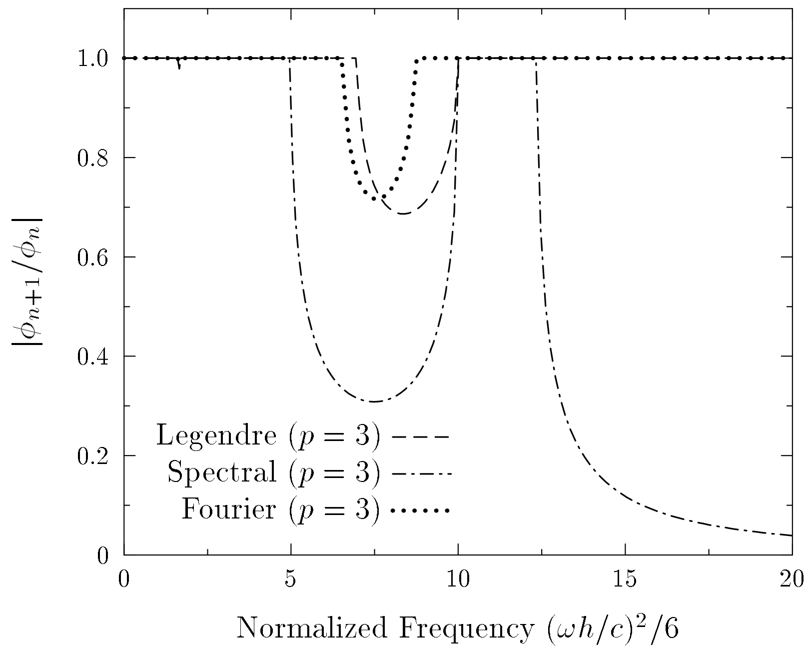

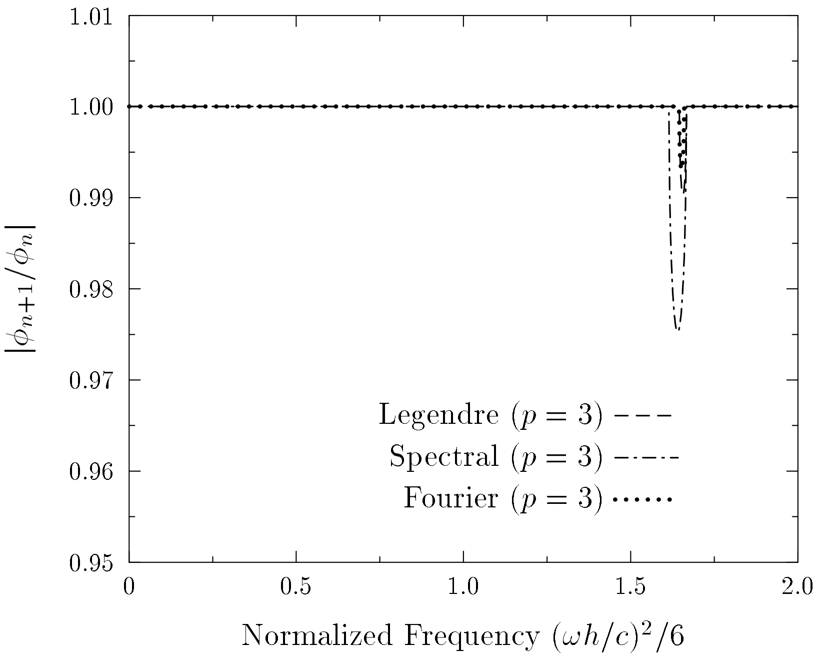

Figure 9.5: (Top): Amplitude spectrum for cubic elements. (Bottom): Isolation of amplitude spectrum near first complex wavenumber band.

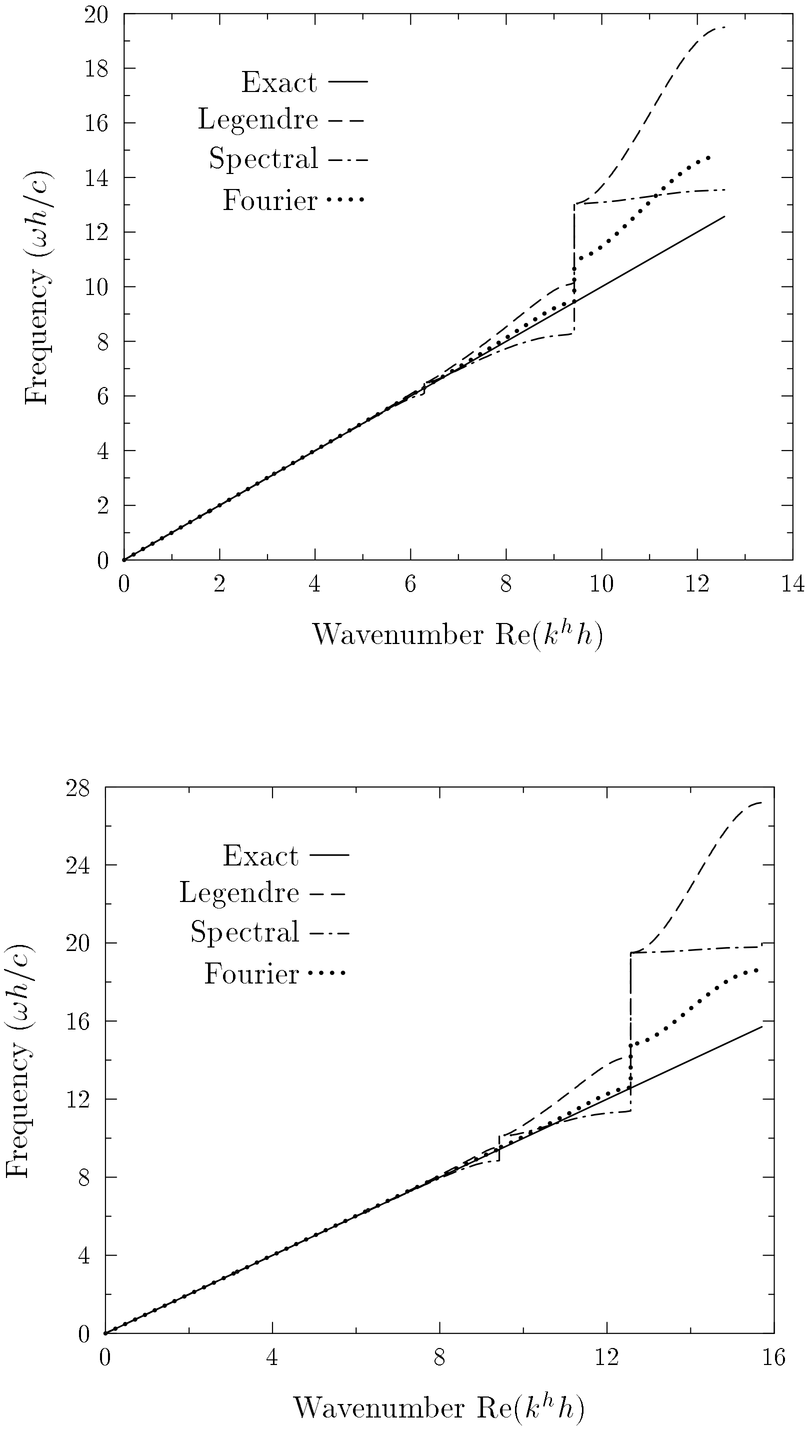

Figure 9.6: Frequency spectrum for spectral orders, (Top): $p = 4$ (Bottom): $p = 5$. Results shown for real wavenumbers only.

elements exhibit loss of accuracy in the upper two optical branches. In contrast, the Fourier element maintains accuracy up to $\alpha = (p-1)\pi$.

In conclusion, the following dispersive properties are observed: (1) There are p passing bands and p stopping bands, (2) the limit of resolution occurs at $Re(\beta) = \pi p$. In addition, *the amplitude attenuation in the first few complex wavenumber (stopping) bands is very small and converges in the limit of large spectral orders to the exact amplitude ratio of one. Thus for large spectral orders the first few stopping bands are not of practical significance.* As a general trend we observe that the amplitude error is greater for the Spectral elements than the Legendre and Fourier elements and the cutoff for Spectral elements always occurs before that of Legendre elements.

9.6.3 Analysis of phase error

Figure 9.7 shows the phase accuracy of the Galerkin finite element approximation versus a nondimensional real wavenumber $(\beta/\pi p)$. The wavenumber is divided by the spectral order p to obtain an equitable comparison between the methods with the same number of degrees of freedom per wavelength. Throughout the acoustic branch, the phase error converges to the exact solution as the spectral order is increased. Clearly, in the practical range $0 \leq k^h h/\pi p \leq .5$ the higher-order p–type elements exhibit increased accuracy compared to low-order finite elements, for the same number of degrees of freedom. In the optical branches, the dispersive errors increase. The use of trigonometric shape functions in the Fourier elements decreases the phase error found in the optical branch as compared to the Legendre case.

The spectral convergence rate of the phase error is observed by fixing the nondimensional wavenumber at $kh/p = \pi/5$. This wavenumber corresponds to ten elements per wavelength divided by the spectral order. The results are given in Table 9.1 for Legendre and Spectral elements up to order $p = 5$. Results for Fourier elements are similar to Legendre elements.

The convergence rate of p–type elements is investigated further by examining the phase as the number of solution variables per wavelength is increased. For example for $p = 1$ a Taylor series expansion of the dispersion relation (9.40) gives,

$$k^h h = \alpha \pm \frac{(\alpha)^3}{24} + \frac{3(\alpha)^5}{640} \pm \mathcal{O}(\alpha)^7 \tag{9.49}$$

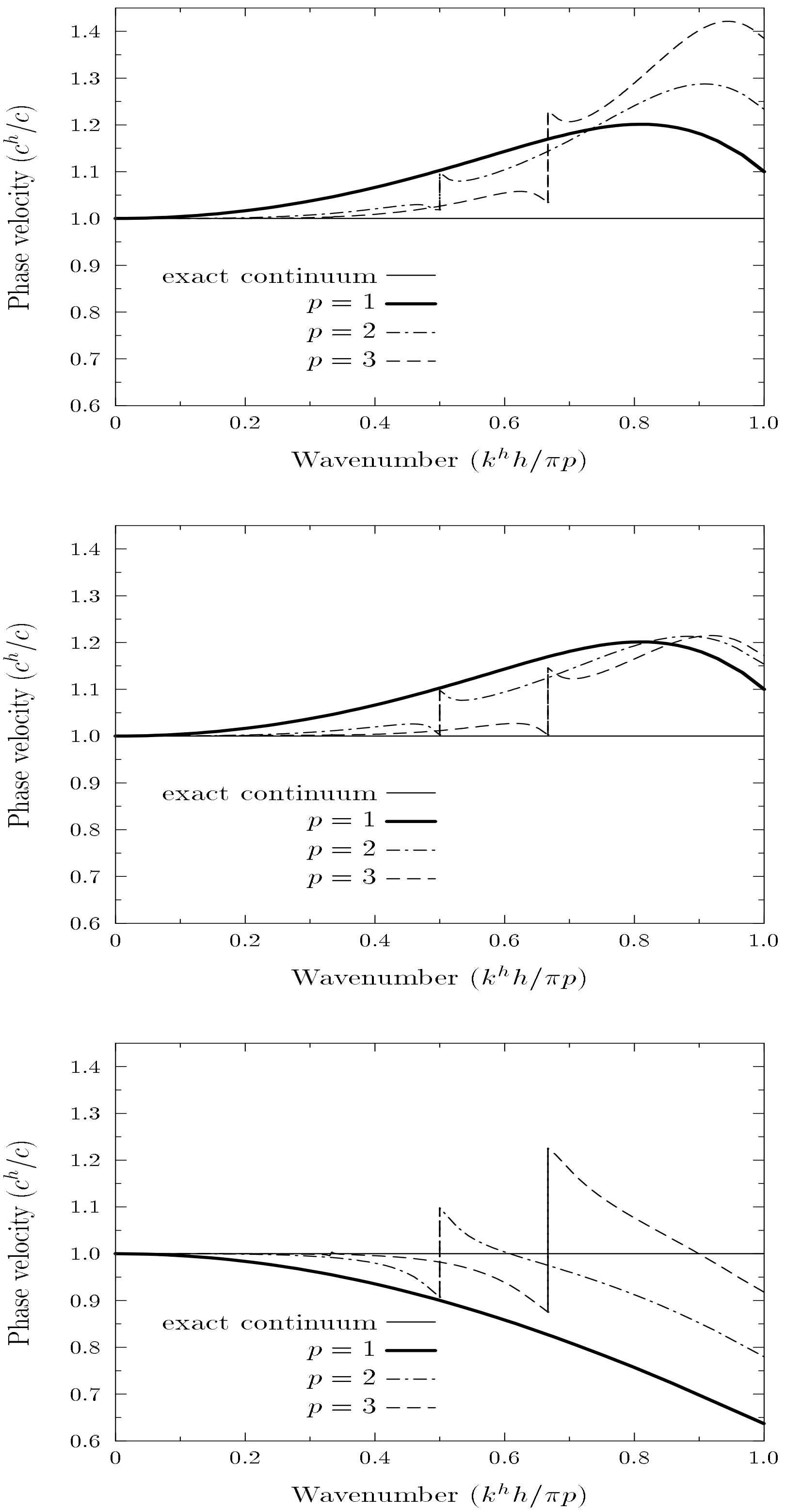

Figure 9.7: Phase velocity error for spectral orders $p = 1, 2, 3$. (top) Legendre basis, (middle) Trigonometric basis, (bottom) Spectral basis.

Table 9.1: Phase error (percent) for fixed $kh/p = \pi/5$

p	Legendre	Spectral
1	1.60e-00	-1.69e-00
2	1.59e-01	-9.17e-02
3	1.96e-02	-7.50e-03
4	2.63e-03	-9.60e-04
5	3.69e-04	6.58e-03

where the plus sign is for diagonal mass and the minus sign for consistent mass. From this expansion it is found that the finite element nodal solution is locally second order accurate. In general, in the range of resolution, the phase error for spectral order p is of the order,

$$\frac{k^h}{k} - 1 = \mathcal{O}(kh)^{2p} \tag{9.50}$$

with the nodal solution,

$$\boxed{\phi_n = A\mathrm{e}^{ikx_n[1 \pm \mathcal{O}(kh)^{2p}]}} \tag{9.51}$$

This result is verified for spectral orders of $p = 1, 2, 3$ in Figure 9.8, where the slope of the lines show the rate of convergence of the phase error to be $2p$. For reference, we note that 10 elements per wavelength corresponds to -1.0 on the abscissa of this plot.

9.6.4 Analysis of attenuation

Although the amplitude from node to node is exact for frequencies within the passing bands, it is possible for the high-order finite element solution to exhibit amplitude attenuation at points internal to physical nodes. Analysis of amplitude attenuation at points internal to the physical nodes is investigated by examining quadratic elements of order $p = 2$. In this case, the dynamic stiffness matrix is assembled without condensation and the internal variable is written in terms of the center point. The resulting stencils related to equations n and $n \pm 1/2$ are of the form,

$$S(\alpha) = 0 \tag{9.52}$$

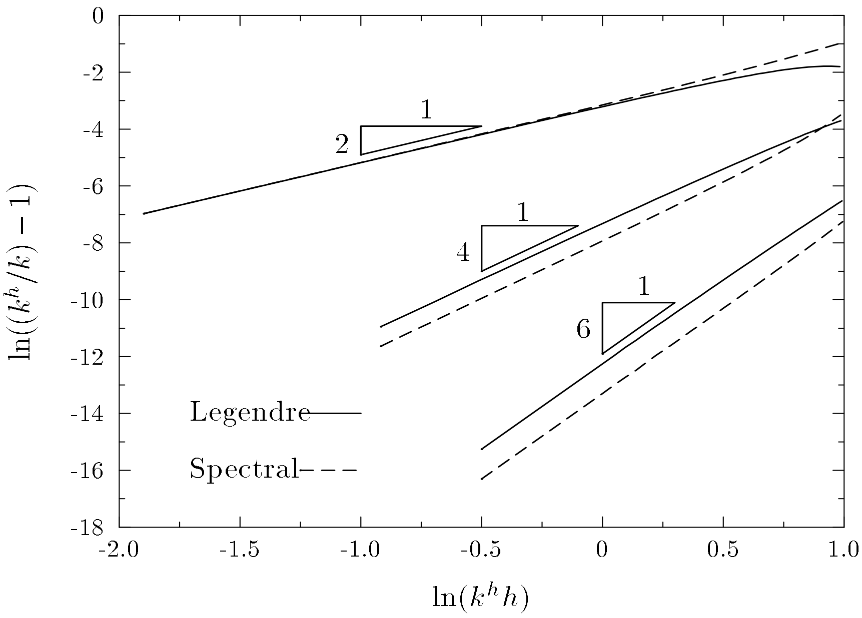

Figure 9.8: Convergence of phase error with polynomial orders $p = 1, 2, 3$.

where

$$S(\alpha) := (K - \alpha^2 M) \tag{9.53}$$

and K and M are (2×5) stiffness and mass coefficient matrices, with solution vector,

$$\boldsymbol{\phi}^T = \left(\begin{array}{ccccc} \phi_{n-1} & \phi_{n-1/2} & \phi_n & \phi_{n+1/2} & \phi_{n+1} \end{array} \right) \tag{9.54}$$

Allowing for different amplitudes at the exterior nodes n, and element center nodes $n \pm 1/2$ we assume the complex exponential solutions,

$$\phi_n = A_1 \mathrm{e}^{i\beta(n)} \tag{9.55}$$

$$\phi_{n+1/2} = A_2 \mathrm{e}^{i\beta(n+1/2)} \tag{9.56}$$

Substitution of the above two solutions into (9.52) results in the symmetric characteristic matrix,

$$\widetilde{S}(\alpha, \beta) = \left[\begin{array}{cc} \widetilde{S}_{11} & \widetilde{S}_{12} \\ \widetilde{S}_{12} & \widetilde{S}_{22} \end{array} \right] \left\{ \begin{array}{c} A_1 \\ A_2 \end{array} \right\} = \mathbf{0} \tag{9.57}$$

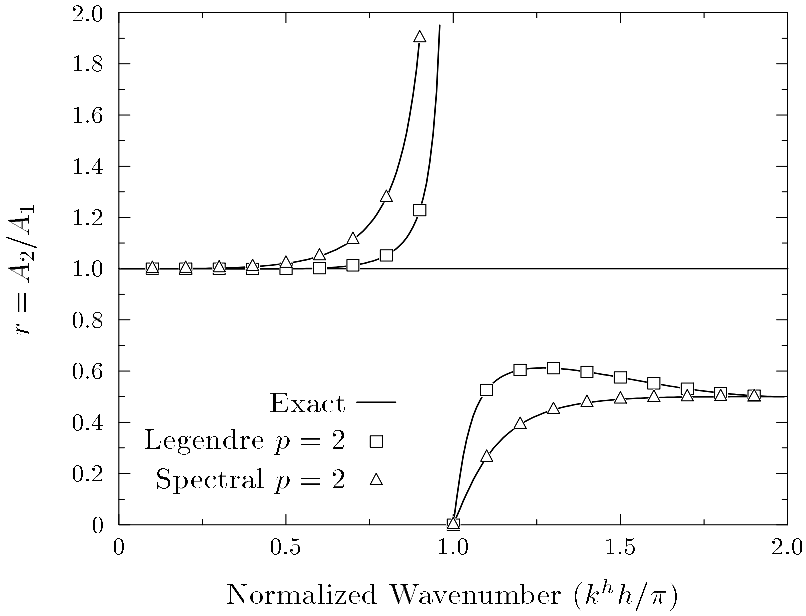

Figure 9.9: Amplitude spectrum for quadratic elements at interior nodes

Solving this system, the amplitude ratio $r = A_2/A_1$ is,

$$r(\alpha, \beta) = -\frac{\widetilde{S}_{12}(\alpha, \beta)}{\widetilde{S}_{22}(\alpha, \beta)} = -\frac{\widetilde{S}_{11}(\alpha, \beta)}{\widetilde{S}_{12}(\alpha, \beta)} \tag{9.58}$$

Note that the dispersion relation found earlier in (9.40) is obtained by setting the characteristic matrix to zero, $\det \widetilde{S} = \widetilde{F}(\alpha, \beta) = 0$.

Figure 9.9 shows the amplitude ratio $r = A_2/A_1$ plotted as a function of wavenumber. The curves lying above the ratio of one are acoustical branches, while those below are optical branches. In the range $0 \leq \beta \leq 2\pi/3$, the amplitudes are nearly equal to the exact value of one. Near the stopping band, $\beta = \pi$, r increases rapidly. At $\beta = \pi$, the amplitude ratio skips to the optical branch where it assumes the value zero. In the optical branch the ratio tends to the limit $r = 0.5$. The physical interpretation of this result is discussed at length in BRILLOUIN [1953]: Here we emphasis that two alternative interpretations are possible: (i) Referring to (9.56), the solution for the finite element mesh can be represented as *two waves*, one propagating along the exterior nodes n, and the other propagating along the interior points $n \pm 1/2$. (ii) An alternative representation is a *single wave* propagating through both interior and exterior points,

$$\phi_m = C_+ e^{i(\bar{\beta})m} + C_- e^{i(\bar{\beta}-\pi)m} \tag{9.59}$$

where $\beta = 2\bar{\beta}$ and $C_+ = (A_1 + A_2)/2$ and $C_- = (A_1 - A_2)/2$. This solution describes the superposition of two waves propagating in opposite directions with wavenumbers $\bar{\beta}$ to the right and $\bar{\beta} - \pi$ to the left. The wave propagating to the right is partially reflected as it traverses each node, thus giving rise to a solution that consists of both a transmitted and a reflected wave component. The physical significance of this result is that while the amplitude is exact from node to node for frequencies within passing bands, the reflected wave component causes amplitude attenuation at internal points.

For quadratic Legendre elements, amplitude attenuation is insignificant for $k^h h < 2\pi/3$ (three elements per wavelength), while for quadratic Spectral elements amplitude attenuation is insignificant for $k^h h < \pi/2$ (four elements per wavelength). Results for Fourier elements are similar to the Legendre elements.

9.7 Frequency response spectrum

The role that complex wavenumbers play in the practical solution of physical boundary value problems is revealed in the time-harmonic solution for the Helmholtz equation with Dirichlet boundary conditions $\phi(0) = \bar{\phi}$ and $\phi(L) = 0$, where L is the length of the domain. After discretizing with N uniformly spaced elements of length h, it can be shown that the finite element solution is,

$$\phi^h(x_n, \omega) = \bar{\phi}\frac{\sin(k^h(L - x_n))}{\sin(k^h L)} \qquad n = 0 : N \tag{9.60}$$

where k^h is the numerical wavenumber defined in (9.40) and $L = Nh$ and $x_n = nh$. The important point here is that this wave solution consists of the same numerical wavenumbers present for the infinite domain found by our Fourier analysis except that both outgoing and incoming waves are present.

The existence of the cut-off frequency and stopping bands for the example problem is exposed from the frequency response spectrum. Figure 9.10 shows the frequency response at the midnode for a uniform mesh of ten quadratic ($p = 2$) elements.

$$R(\omega) = \phi^h(x_5, \omega)/\bar{\phi} \tag{9.61}$$

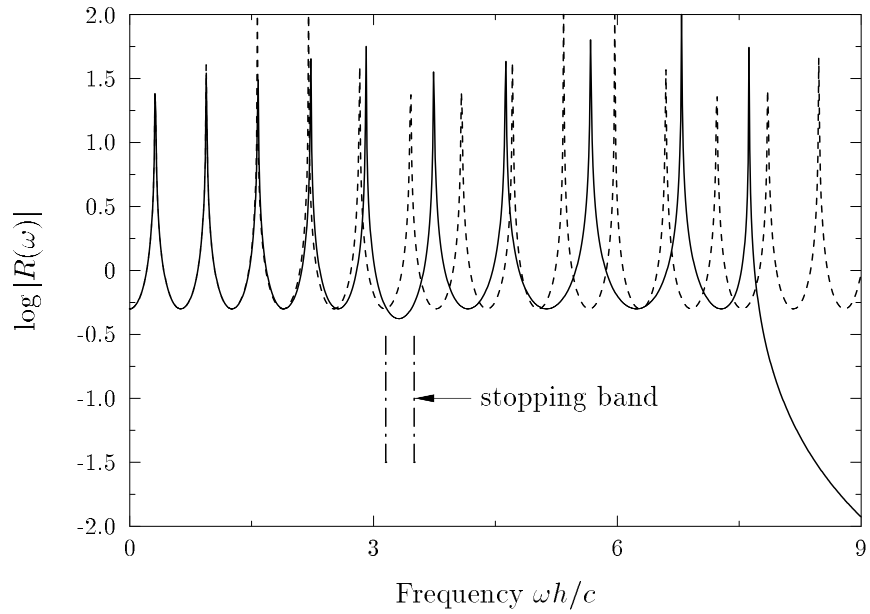

Figure 9.10: Frequency response spectrum for example problem using 10 quadratic Legendre elements.

The sharp peaks indicate the position of the resonant frequencies of the vibration problem. Accurate results are obtained throughout the acoustic branch while considerable errors are present in the optical branch. The existence of the stopping band (complex wavenumber band) is evident by the decrease in amplitude response at $(\omega h/c) \approx \pi$.

In Figure 9.11, the response for a frequency in the stopping band is plotted. It is clear that the response has a propagating component fixed at $Re(k^h h) = \pi$ corresponding to two elements per wavelength, while the imaginary component manifests itself in the amplitude decay. Further results can be found in THOMPSON AND PINSKY [1993a,b].

9.7.1 Discrete eigenvalues

For the example problem, the exact eigenmodes $k_j = j\pi/L, j = 1, 2, \cdots \infty$ are linearly proportional to the eigenvalues through the characteristic relation $\omega_j h/c = k_j h$. It can be shown that the real eigenmodes for a uniform mesh of finite elements of any spectral order are,

$$k_j^h = j\pi/L \qquad j = 1 : pN - 1 \tag{9.62}$$

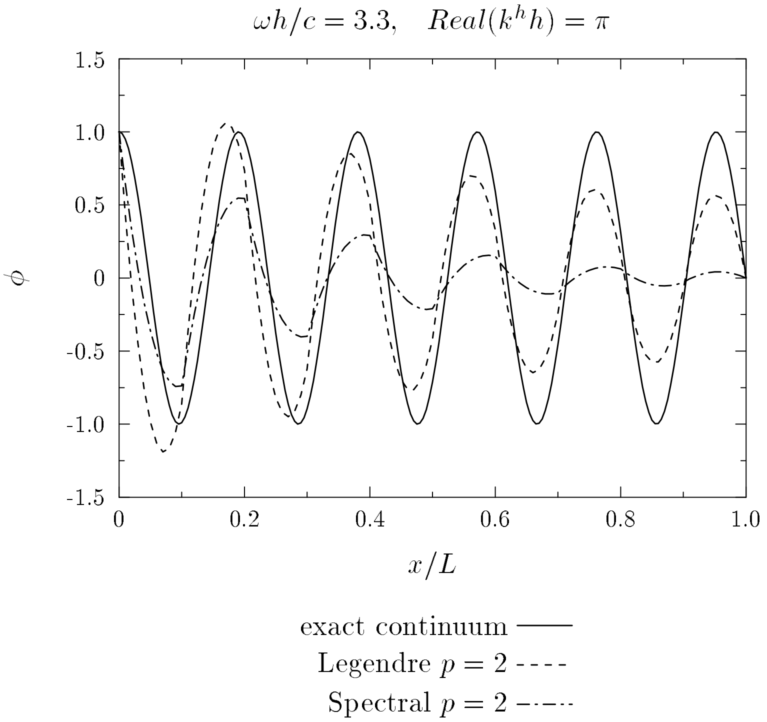

Figure 9.11: Harmonic decaying wave solution for example problem for a driving frequency in the stopping (complex wavenumber) band.

Thus the eigenmodes for the finite element mesh are exact, up to the number of free variables $(pN-1)$ present in the mesh. Discrete eigenvalues $\omega_j h/c$ are calculated from the dispersion relation (9.40) in which real frequency roots are sought for the given real eigenmodes $k_j h$. The result is a characteristic polynomial in $\alpha_j = \omega_j h/c$ of order $2p$.

$$\sum_{l=0}^{p} c_l \alpha_j^{2l} = 0 \tag{9.63}$$

For quadratic Legendre elements, the characteristic equation and its roots are,

$$\boxed{c_o + c_1\alpha_j^2 + c_2\alpha_j^4 = 0} \tag{9.64}$$

where

$$\begin{aligned} c_0(k_j h) &= 20(1-\cos k_j h) \\ c_1(k_j h) &= -2(13 + 2\cos k_j h)/3 \end{aligned}$$

$$c_2(k_j h) = (3 - \cos k_j h)/12$$

$$\left(\frac{\omega_j h}{c}\right)_1^2 = \frac{-c_1 - \sqrt{c_1^2 - 4c_0c_2}}{2c_2} \tag{9.65}$$

$$\left(\frac{\omega_j h}{c}\right)_2^2 = \frac{-c_1 + \sqrt{c_1^2 - 4c_0c_2}}{2c_2} \tag{9.66}$$

For a uniform mesh with $N = 10$ quadratic elements, there are nineteen discrete frequencies corresponding to nineteen active degrees-of-freedom. These frequencies are calculated from (9.65) and (9.66) and are plotted as tick marks on the dispersion curves in Figure 9.2a. We note that the second root (9.66) corresponds to the upper branch (optical branch). At the stopping band $k_j h = \pi$, there is a discontinuity in the frequency/wavenumber relation, where there are two possible choices for the roots. Eigenfrequencies in the range between these roots are skipped over. From numerical results, it was found that the eigenfrequency occupies the lowest energy mode at this wavenumber and falls on the smaller of the two roots. The discrete eigenfrequencies fall exactly on these dispersion curves; below the cut-off frequency and outside the stopping band. These results demonstrate that the real part of the complex wavenumber Fourier analysis accurately predicts the discrete eigenfrequency spectrum.

9.7.2 Post-processing of eigenmodes

The eigenvectors for the example problem are,

$$\sin(k_j x_n) = \sin(j\pi x_n/L) \qquad j = 1 : pN - 1 \tag{9.67}$$

Comparing this result to the analytical eigenfunctions, the eigenvectors are nodally exact for all spectral orders. Figure 9.12 shows an example of mode j=18 representing a wavenumber in the upper optical branch of a uniform mesh of ten quadratic elements. At the nodal points n, the amplitude A_1 is exact, whereas at the intermediate points $n \pm 1/2$ the amplitude A_2 is given by the ratio $r = A_2/A_1$ defined earlier in Figure 9.9. For mode $j = 18$, there are two aliased wave solutions, one passing through each set of points n and $n \pm 1/2$,

$$\phi_n = A_1 \sin(\beta_2 n) \qquad n = 0 : N \tag{9.68}$$

$$\phi_{n+1/2} = A_2 \sin(\beta_2 (n + 1/2)) \qquad n = 0 : N - 1 \tag{9.69}$$

where $\beta_2 = (2\pi - \beta_{18}) = \pi/5$, see Figure 9.13.

Using information obtained from the complex Fourier analysis, mode shapes for higher-order elements can be processed in order to isolate individual wave components. By superposition of these wave components, a single wave solution can be constructed with a global sinusoidal interpolation. The global sinusoidal interpolation of nodal data improves the representation of the eigenmode at inter-nodal points.

For example, for mode $j = 18$, by applying a discrete sine transformation BELLANGER [1989] with sample points ϕ_m, i.e.

$$w_j = \frac{1}{N} \sum_{m=1}^{2N-1} \phi_m \sin(\frac{jm\pi}{2N}), \qquad j = 1 : 2N - 1 \tag{9.70}$$

we find that the only nonzero wave amplitudes are w_2 and w_{18} illustrated in Figure 9.14. Using the inverse sine transform,

$$\phi_m = \sum_{j=1}^{2N-1} w_j \sin(\frac{jm\pi}{2N}) = w_2 \sin(\frac{m\pi}{10}) + w_{18} \sin(\frac{9m\pi}{10}) \tag{9.71}$$

we then superimpose these two wave components to form the single wave constructed from the sinusoidal interpolation,

$$\boxed{\phi(x) = \sum_{j=1}^{2N-1} w_j \sin(\frac{j\pi x}{L})} \tag{9.72}$$

see Figure 9.15. Comparing this interpolated solution to the imaginary part of (9.59) we recognize the two wave amplitudes as $w_2 = C_+$ and $w_{18} = C_-$. Although the amplitude of the sinusoidal interpolation of the eigenmode is attenuated, the post-processed eigenmode better represents the exact sinusoidal mode shape – compare Figure 9.12 and 9.15.

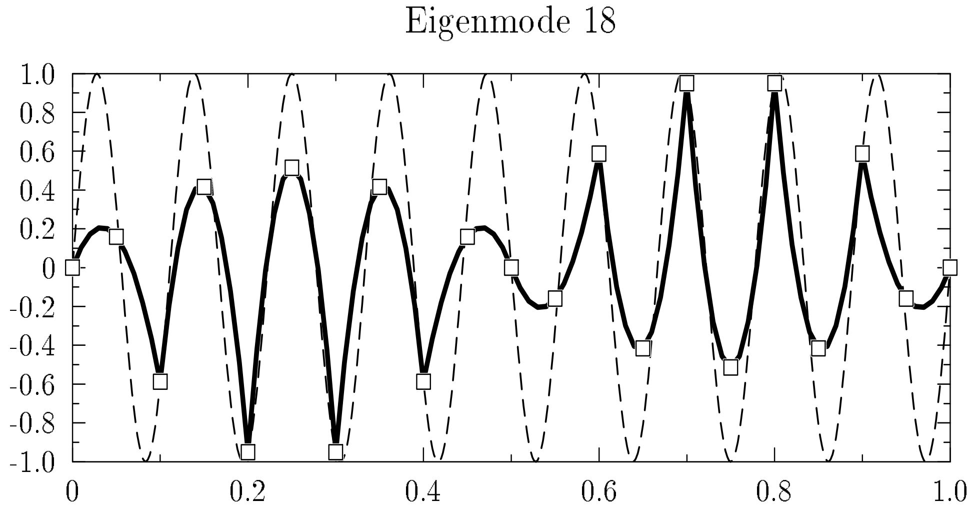

Figure 9.12: Mode shape $j = 18$ for uniform discretization of ten quadratic Legendre elements. The dashed curve denotes the exact mode while the solid line denotes the approximate mode interpolated with quadratic shape functions. The square tick marks denote nodal values.

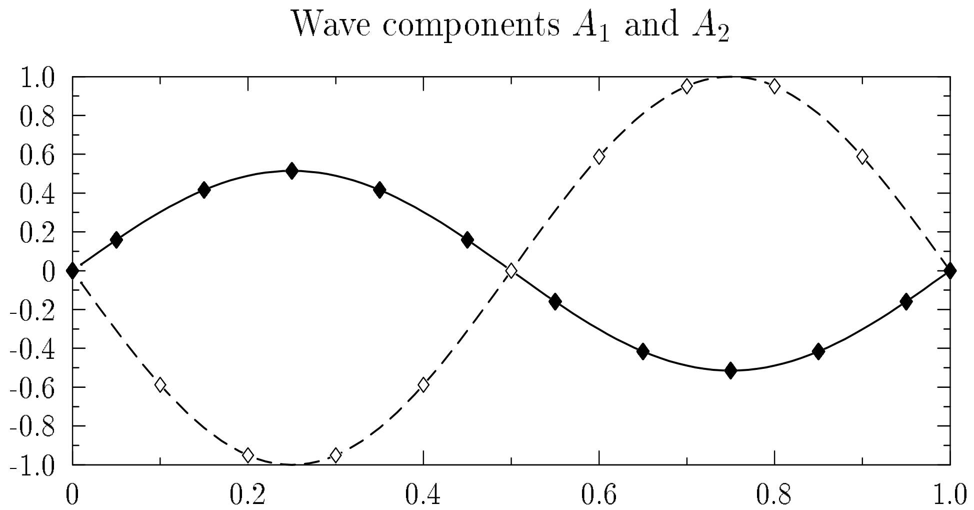

Figure 9.13: Two aliased wave solutions for mode $j = 18$; one passing through each set of points n and $n \pm 1/2$. Dashed curve indicates wave component A_1 while the solid curve indicates A_2.

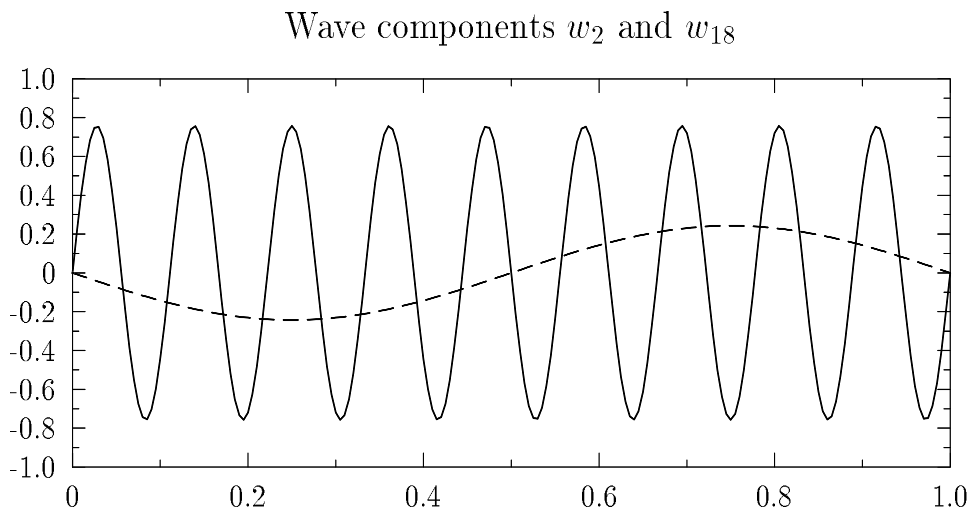

Figure 9.14: Two wave components obtained from discrete sine transform of mode $j = 18$. Dashed curve indicates wave component w_2. Solid curve indicates w_{18}.

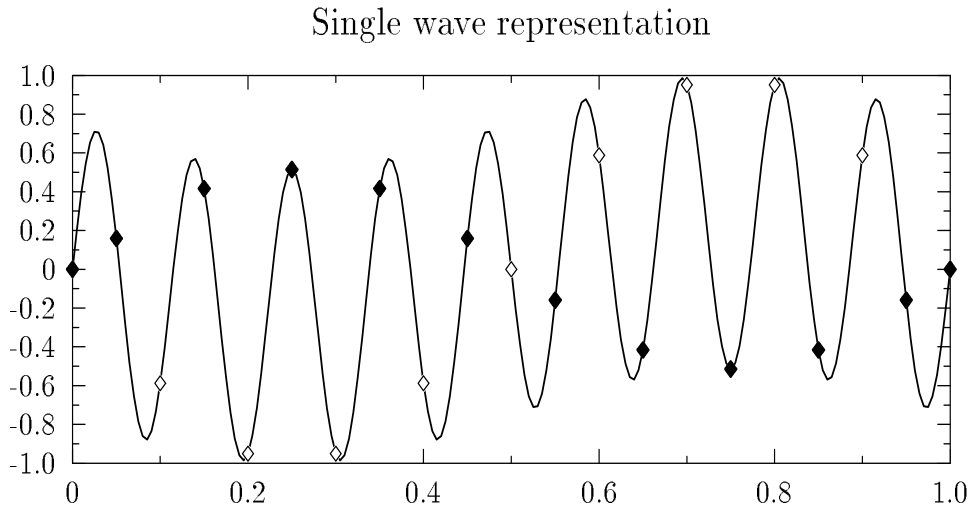

Figure 9.15: Processed mode shape: Sinusoidal interpolation for mode $j = 18$.

9.8 Summary and Conclusions

In this chapter we have shown that high-order finite element discretizations display frequency bands where the solutions are harmonic decaying waves. In these so called 'stopping' bands, the solutions are not purely propagating (real wavenumbers) but are attenuated (complex wavenumbers). In order to interpret the solution within the stopping bands the standard finite element dispersion analysis technique has been extended to include complex wavenumbers. By allowing for complex wavenumbers, a complete characterization of the stopping bands in the frequency spectrum of high-order finite element discretizations has been obtained.

The most important conclusions from this study are summarized as follows:

1. There are p stopping bands present in the dispersion curves of p–type elements

2. For large spectral orders p, the width of the first few stopping bands are very small and the amplitude attenuation is minimal. Thus for high-order finite element basis functions, the first few stopping bands are not of practical significance.

3. High-order elements display increased phase accuracy compared to low-order elements for the same number of degrees of freedom. For example, for linear elements ($p = 1$), a practical limit on phase accuracy is to require at least ten elements per wavelength. For quadratic elements ($p = 2$), as few as three quadratic elements per wavelength are required to obtain accurate phase. For a spectral order of ($p = 3$), only two elements per wavelength are needed to maintain phase accuracy. To resolve waves with increased accuracy while maintaining only two elements per wavelength, spectral orders of ($p \geq 4$) are recommended.

4. For well resolved waves, spectral elements using Lagrange interpolation in conjunction with Lobatto quadrature give improved convergence rates for phase error when compared to hierarchic elements with either Legendre or Fourier basis functions.

5. For nondimensional frequencies extending beyond the recommended limits, both dispersion and amplitude attenuation errors increase the most for spectral elements.

6. For nondimensional frequencies in the upper branches of the frequency spectrum, hierarchic p-type elements with Legendre basis exhibit improved amplitude accuracy over the spectral elements, while the new hierarchic Fourier elements exhibit improved accuracy for both amplitude and phase.

A study of the closed form solution for a canonical steady-state vibration problem demonstrated the role complex wavenumbers play in the finite element solution of boundary value problems. Frequency response results clearly display the existence of the cut-off frequency and stopping bands present in the finite element solution. The important point here is that finite element solutions to vibration problems are composed of the same numerical wavenumbers found in the complex Fourier analysis except that both outgoing and incoming waves are present. In addition there is a direct connection between the dispersion curves (real part of the complex wavenumber characteristic relation) and the discrete eigenvalue spectrum for the vibration problem. In this case, all eigenmodes correspond to real wavenumbers, and thus the real eigenvalues (eigenfrequencies) all fall below the cut-off frequency and outside the stopping bands.

In the later part of this chapter we have shown how p–type finite element solutions to vibration problems can be post-processed using information obtained from the complex wavenumber Fourier analysis. Complex wavenumber analysis allows for the determination of the underlying component waves. By superposition of these wave components through a sinusoidal interpolation, a better approximation for the mode shape at inter-nodal points can be constructed. This process demonstrates how results from a complex wavenumber Fourier analysis can be used as a tool to help improve finite element solutions to vibration problems.